Department of the Navy
Office of Naval Research
Contract N6onr-244 Task Order II
NR 062-010

EXPERIMENTAL STUDY OF FLOW BETWEEN CENTRIFUGAL PUMP SHROUDS

H. N. Tyson, Jr.

Hydrodynamics Laboratory
California Institute of Technology
Pasadena, California

Project Supervisor:
A. J. Acosta

Approved by:
A. Hollander

Report No. E-19.6

July 1954

Abstract

An experimental investigation of flow between the shrouds of an impeller has shown that gross flow separation can occur for "well designed" shapes. Rotation of the shrouds inhibits separation and if the flow coefficient is sufficiently low it will be completely prevented.

For the particular impeller shroud profile studied it was found that the velocity distribution in the inlet regions (near where the impeller inlet edge would be placed) is satisfactorily approximated by potential theory. Potential flow velocity distributions on several families of shroud shapes suitable for impeller or supercharger design are then given for use in design.

I. Introduction

This report is part of a continued effort to obtain detailed information on internal flow phenomena in turbomachine impellers. Previous studies[1-6] undertaken at this Laboratory have shown the need for further investigations of the flow through the inlet portions of the impeller. It is known[6] that a substantial proportion of the hydraulic losses within "Francis"-type impellers may be due to a sudden expansion or deceleration of the flow near the vane inlet. These losses are important and may be further increased by the possibility of complete flow separation from the suction shroud because of the relatively small radius of curvature there.[5]

The design operating condition or best efficiency point and cavitation susceptibility of a pump are governed to a considerable extent by these losses, at least for Francis-type impellers. Lower specific speed impellers are probably not as sensitive to inlet performance because of the larger skin friction losses encountered in the impeller passages and the lower flow rates used. Inlet losses arise from the deleterious effects of poor shroud design and from the incorrect vane inlet design resulting from the lack of knowledge about shroud effects. For example, it is usually assumed in commercial practice[7, 8] that the meridional

velocity is constant across the shroud channel cross sections. There is no doubt that due to the curvature of the flow some variation of velocity exists. Thus designs based upon this assumption must be in error to some extent.

These remarks have indicated the reasons and general desirability for making such an investigation. A program was accordingly laid out to determine the internal velocity distributions in the shroud passage of a well-designed commercial impeller of the Francis type. In order to simulate the operating conditions of the pump as well as possible, the shrouds are rotated to correspond to various flow rate coefficients. These measurements are then compared to calculations based on potential theory, to show whether or not such an analysis is useful for design purposes. Lastly, shroud velocity distributions determined by electrical analogy are presented for several families of transition shapes.

II. Description of Laboratory Facilities

A detailed description of the laboratory facilities may be found in Refs. 1 and 2, so that only a few of the more important features will be mentioned here. The test facility consists essentially of a closed hydraulic circuit using water as the fluid medium, with a circulating pump, Venturi flow meters, and a system of piping to distribute the flow to any of three test sections in which experimental models can be installed. The circuit can be arranged so that the flow can approach the test section in either direction.

The test section used for the present work was provided with one-half horsepower "V"-belt impeller drive. The flow was delivered to the impeller shrouds via an approach section in which a honeycomb flow straightener had been installed five diameters upstream, and it discharged from the shrouds into an open cylindrical basin. A return line then led the flow back to the sump. The water free surface in the test basin was maintained slightly above the level of the shrouds during operation. The flow was regulated by a manual throttle valve and speed-controlled circulating pump. The shroud rotative speed was determined by means of a General Radio Corporation Type 631-B "Strobotac". In this way the flow and shroud rotative speeds were maintained to within one-half and one percent of their nominal settings, respectively.

The assembled impeller shrouds and drive mechanism are shown in Fig. 1. A pair of stationary annual disc diffusor plates serve to keep the flow parallel for a short distance outside the shrouds.

a. The Impeller Shrouds

The impeller shrouds used for the present series of experiments were made of lucite and were scaled from one of the Grand Coulee pump impellers[2] since considerable other detailed information is available on this design.[1, 2, 6, 8] A definition sketch of the impeller shrouds is shown in Fig. 2.

b. Instrumentation and Experimental Procedure

The following experimental observations were made in this work: (a) the measurement of the pressure on the impeller shroud surfaces; (b) the measurement of the velocity and total head distributions across the shroud profile at two stations (see Fig. 2), and (c) a visual study of flow separation within the impeller shrouds. Each of these tests was done for various rates of rotation of the shroud. For ease of instrumentation only the suction shroud was rotated in obtaining all observations, except for pressure distributions on the suction shroud itself.

The distribution of pressure along the shroud profile was determined by means of twelve piezometer taps (0.03 in. diameter) placed on each shroud at various radial positions. The pressure signals along the back shroud were measured relative to the static head at the throat of the inlet nozzle with a bank of simple air-water manometer tubes connected to a common manifold.

In obtaining the pressure distribution on the suction shroud, both shrouds were fastened together so that they turned as a unit. Customarily, the measurement of pressure signals on a rotating device requires a system of complicated rotating seals from which the pressure signal is led to a stationary manometer bank. The complexity of such a system was circumvented in the above case with the use of a circular multitube manometer, rigidly attached to the back shroud (see Fig. 1), and rotated with it. The manometer was mounted concentrically with the axis of the shrouds, and was equipped with thirty 5 mm. glass tubes 18 in. in length leading to a common manifold. The manifold was split so that the range of the

measurable pressure differential might be doubled. The manometer readings were observed with the aid of a synchronized strobolight. The distribution of pressure on the shroud was found from the readings by accounting for the centrifugal force field.

The internal velocity surveys at stations $\overline{AB}$ and $\overline{CE}$ (Fig. 2) were made by means of several probing devices. Since the meridian velocity profile was to be investigated as a function of the flow coefficient, it was necessary to measure the direction as well as the magnitude of the velocity. For example, the fluid particle velocity at the suction shroud was tangential and had the local shroud rotative speed, whereas near the top shroud the flow was radial. To measure the flow angles across the passage, a claw probe (Fig. 3-b) was used with a holding device (Fig. 3-a), constructed so that the probe could be positioned radially and angularly in the passage to within at least 0.02 unit passage widths and $1/4^{\circ}$, respectively. The flow angle could be measured to within $\pm 1^{\circ}$ in most cases, but at certain values of ϕ the accuracy was reduced by large flow fluctuations. The claw probe was calibrated in an air jet of a large contraction ratio nozzle.

Once angle determinations across the passage were made, total head and static surveys could be done. Three types of probes were used for this purpose (Fig. 3-b); the Venturi type total head probe for general use, a static head probe, and a special boundary layer total head probe for use in close proximity to the suction shroud.

To measure the probe pressure signals a 0-0.1 psi Statham (P5-0.1D-125) differential pressure electric strain gauge was used in conjunction with a Baldwin Southwark resistance bridge.

In order to effect a visual study of the separation phenomenon in the flow through the shrouds, small easily identified immiscible globules (dibutyl phthalate and kerosene) of unit specific gravity were released from a tube in the throat of the inlet nozzle. The flow was varied over a range of Reynolds numbers, based on inlet diameter and mean velocity, and the suction shroud rotative speed sufficient to suppress separation at the shroud exit was recorded.

III. Experimental Results

a. Flow Separation

Gross flow separation in the passage was evidenced by back flow of the tracer particles. For a given flow rate (or Reynolds number) the extent of separation was seen to decrease with increasing angular speed ultimately resulting in no separation at all. The inception of separation was said to occur when the tracer bubbles at the exit of the shroud shape (point B in Fig. 2) just indicated no back flow. From these observations the flow coefficient necessary to suppress separation was plotted as a function of Reynolds number based on the inlet diameter (Fig. 4). This critical value of flow or speed coefficient should approach an asymptotic limit as the Reynolds number becomes large. Limitations of speed prevented determining this value accurately, but from Fig. 4 it is probably about $\phi = 0.20$.

b. Shroud Pressure Distribution

Because of the large real fluid effects noted above, there is no doubt that velocity and pressure distributions will depend on the operating point and differ markedly from ideal fluid calculations. That this is the case is evident in the plot of back shroud pressure distribution vs. flow rate coefficient (Fig. 5). For high values of ϕ the flow is separated and this is reflected in the low values of pressure coefficient obtained at the impeller discharge. With an increase in rotative speed, the separated regime decreases in extent and the pressure increases ultimately to a value slightly greater than indicated by potential flow. This change is observed likewise on the rotating suction shroud (Fig. 6). Due to the fact that the readings were small and the possibility of error correspondingly large, considerable scatter is shown near the impeller exit for these curves.

It is clear from both of these figures that separation occurs somewhat behind the minimum pressure point on the suction shroud near the survey point "E". The pressure distributions from this point upstream do not differ substantially from the perfect fluid calculations, a fact which makes them useful for design.

c. Meridional Velocity Distribution

The general observations noted above are borne out by the velocity profile measurements shown in Fig. 7. Figure 7a is the velocity profile a short distance ahead of the impeller. The internal survey midway through the impeller (station C-E) and at the exit (station A-B) both show separated profiles and their subsequent stabilization by shroud rotation. It should be mentioned at this point that marked flow asymmetries occurred when the flow was detached from the lower shroud. For that reason the meridian velocity profiles at the exit are scaled, so that they each have the same mean values, and in this way the profile shape is readily seen as a function of operating point.

Energy distributions at the two internal stations are shown in Fig. 8 as a function of flow rate. It is immediately seen that as the flow coefficient decreases, the boundary layer defect is increasingly offset by energy input from the rotating shroud. The extent of the affected region is also given in Fig. 10, in which the flow direction is given. The total head coefficient ζ is the difference between the total head at any point and the inlet static pressure. A true loss coefficient may be obtained by subtracting off the inlet total head coefficient.

A static pressure survey is shown for station C-E in Fig. 9. The experimental data may be compared with the potential flow calculations which are shown as a dashed line. The discrepancy at $\phi = \infty$, i.e., no rotation, is due to flow asymmetry at this operating point. Although shroud rotation significantly stabilizes these asymmetries, they still persist to a slight extent for all flow rates.

A small obstruction was placed a short distance upstream of the nozzle throat to increase the inlet boundary layer thickness. It was found that this had little or no effect on these results.

IV. Discussion

It is evident from the results that rotation of impeller shroud surfaces substantially restricts boundary layer growth, and can even suppress complete flow detachment. For the present impeller shape, separation was not found to occur below a flow rate coefficient of $\phi = 0.20$. The design point

of the original impeller was $\phi = 0.115$[2] so that there was no danger of gross inlet losses occurring for normal operation. The same cannot be said of lower specific speed impellers, however, in which sharper meridian curvatures are employed. Thus, a very definite possibility of shroud separation may occur, as has been pointed out previously by Gongwer[10] and noted in two-dimensional impeller experiments.[5]

In an actual impeller, the blades if properly designed will tend to assist the boundary layer "centrifuging" associated with operation at moderate flow rates ($\phi = 0.1 - 0.2$). The results of flow separation observations are, then, probably pessimistic, but they stand as safe limits not to be exceeded.

The loss of energy through the impeller was quite small, being on the order of about 0.01 inlet velocity head for flow rate coefficients less than 0.2. For higher flow rates a sharp increase in loss was experienced.

The primary result of this investigation is that the meridian velocity distribution near the region of the impeller vane inlet for practically all flow rates may be approximated closely by potential theory. (The determination of the potential flow is discussed in the following section). This result is apparent from the pressure profiles along the suction shroud (Fig. 6) and in the velocity traverses across the intermediate surveying station (Fig. 7). The disparity that still exists is due to the boundary layer region required at the wall. This defect must be accounted for by an increase in velocity of the main stream. The inlet edges of most impellers lie considerably upstream of the surveying station CE, so that they are in areas less favorable to boundary layer growth. Consequently, one would expect even better agreement with the potential flow results there, provided the oncoming stream was reasonably uniform.

The interest in these results lies in their application to impeller design. The vane leading edge can be designed from a knowledge of the inlet velocity triangle and a theory to account for the finite number of blades. Formulas that consider the latter problem have been given[13] so that only the meridional velocity, wheel speed and pre-whirl, if any, need to be known at any given radius.

Meridian Velocity Distribution

It is evident by now that the usual commercial assumption of constant meridional velocity across the passage[7, 8] can be considerably in error. A comparison of velocity distributions based on potential flow (obtained graphically, see Appendix II) and the standard method (continuity equation) is given in Fig. 14, along various streamlines through the impeller. According to this figure, errors in meridional velocity up to 40% or more may be made. In this figure the arc distance along the particular streamline in question is the abscissa. The points labeled "continuity equation" were obtained by dividing the area formed by the streamline normals into the reference flow rate. This figure gives a somewhat more favorable velocity than would be commercially assumed, because of the different scaling of arc distance along each of the stream lines. There is some discrepancy between the analog and graphical results near the point of tangency of the shrouds with the straight surfaces. Accurate graphical analyses are hard to obtain in this region and so are probably in error here.

Figure 16 shows the meridional velocity distribution across the inlet edge of the impeller[8] together with what would be customarily taken as the meridian velocity there. Because such graphical analyses are time consuming, an approximate velocity distribution obtained with the assumption of a linear variation in radius of curvature is also plotted in Fig. 16. This is easy to obtain (Appendix II) and is fairly close to the more exact solution. However, near regions of sudden change in curvature this approximation is not too good.

It has been shown that appreciable errors in inlet design can occur if account is not taken of shroud curvature. At the present time qualitative information indicates that shockless entry calculations made with proper consideration to the meridian velocity profile and corrections due to a finite number of vanes predict the best efficiency point of the impeller at least on the single impeller studied. The relative importance of these various factors, at least for efficiency, is still an open question. However, there is no doubt cavitation susceptibility is strongly affected by the meridian velocity profile.

Other extraneous effects, such as the inlet volute shape on double suction pumps or operation at low Reynolds numbers, etc., may drastically

change the inlet profile and this work should not be regarded as applicable to these situations. For centrifugal or mixed flow pumps operating at moderate Reynolds numbers ($> 10^5$ say) in configurations where real fluid effectswill not be too large, the application of potential theory will result in inlet velocity profiles useful for design.

In the last section of this report the effect of impeller shroud shape upon meridian pressure or velocity distribution will be determined for several families of designs.

V. Influence of Shroud Transition Curves on Shroud Pressure Distribution

Frequently the flow transition from the axial to radial direction in medium or low specific speed impellers is sudden, often necessitated by space considerations. The resulting underpressures may lead to separation of the flow as seen in the previous sections and possibly cavitation. Thus, a knowledge of the influence of impeller shroud transition curves upon the shroud pressure distribution would be of considerable interest. In addition, a qualitative idea of the shroud velocity distribution near the vane inlet for a given transition curve would make possible a more rapid determination of the meridian flow throughout the passage.

To investigate the influence of various transition curves by construction of several sets of shrouds would be costly. However, since potential theory apparently gives a rather good approximation of the meridian velocity distribution within the shroud passage for flow coefficients typical of most designs and near the inlet particularly, this method would seem expedient and economical. Analyses of this type are often carried out by numerical methods, but they are tedious and time consuming. Since it was desired to obtain the impeller shroud velocity distribution for a number of different transition curves, it was thought easiest to obtain them by means of an electrolytic tank[11]. The use of the electrolytic tank in the solution of potential flow problems is well known. It is easily shown that the electric potential satisfies Laplace's equation in an isotropic conducting medium, under steady state conditions. Likewise, the velocity potential for an irrotational, incompressible flow also satisfies Laplace's equation, and this is the basis of the so-called electric analogy for fluid

flows. Thus measurements of potential gradient in an electrolytic basin are equivalent to determinations of the velocity in a fluid flow provided the boundary conditions are the same.

The electrolytic tank is shown in Fig. 13, as set up for a conical flow. The analog was designed to cover a segment of the surface of revolution. This was done by filling the space between a tilted glass base, the insulator boundaries and the terminal copper plates with the electrolyte, as shown in the above mentioned figure. The center line of the passage is formed by the intersection of the electrolyte free surface with the glass. Full details of the tank design, construction, bridge circuit, and performance are given in Ref. 11.

In order to facilitate a systematic study of the transition curves, the front and back shrouds were represented by a family of simple curves dependent only upon a few parameters. A preliminary survey of radial flow impeller shroud geometries indicated that the front shroud, often made out of circular arcs, can be approximated well by a quarter of an ellipse having its axes parallel to the axial and radial directions (Fig. 14a).

Since the back shroud was more difficult to fit to a simple curve, a separate study was made to determine the effect of the back shroud profile upon the velocity distribution along the suction shroud, the latter being of primary interest. For this study four ellipses of different eccentricity were used as back shroud curves, together with a suction shroud, typical of many pumps. A sketch of the four configurations is shown in Fig. 14b. The ratio of the semi-axes was the only variable and the following values were used:

$$a_1'/a_2' = 0;\quad 0.492;\quad 0.708;\quad 1.000$$

where a_1, a_2 are the semi-axes of the ellipse. The other characteristic lengths were chosen to be similar to those of the shroud profile geometry of Fig. 2; that is,

$$a_1/a_2 = 1.1;\quad r_0/r_2 = 1.9;\quad A_0/A_2 = 1/2\ .$$

Here A_0, A_2 are the inlet and exit areas, respectively; the value of one-half is typical of most Francis-type pumps. In each case the velocity ratio v/v_o is plotted against arc distance divided by the inlet radius r_o measured

from the exit radius. From Fig. 15 it can be seen that, except for the case a_1'/a_2' equal to unity (Curve C_1), maximum velocity on the suction shroud (C_5) is little affected by the shape of the back shroud curve, and the sharpness of the peak of the velocity curve along the suction shroud is only slightly dependent upon the back shroud profile. For simplicity, then, it was decided to use as the back shroud profile an elliptical section centered on the same axes as the suction shroud ellipse (C_3).

With the shape of the back shroud defined, and its effect upon the velocity distribution along the suction shroud determined, it became possible to make a rather systematic investigation of such transition flows.

The outlet to inlet radius ratio (r_2/r_0) was kept constant at a value of 1.9 for all runs. Three different values of the area ratio A_0/A_2 were used and for each of them the suction shroud curvature was varied over a set of values. The table below shows the characteristic proportions for each run:

Table I

Run	r_2/r_0	A_0/A_2	a_1/a_2
1	1.9	1.00	1.0
2	"	"	1.1
3	"	"	1.3
4	"	"	1.6
5	"	0.75	1.0
6	"	"	1.1
7	"	"	1.3
8	"	"	1.6
9	"	0.50	1.0
10	"	"	1.1
11	"	"	1.3
12	"	"	1.6

The back shroud ellipse, defined by a_1'/a_2' (Fig. 14) in each case is obtained from a knowledge of the front shroud shape and area ratio; i.e.,

$$a_1' = r_2; \qquad a_2' = a_2 + b$$

The results of the investigation have been plotted in dimensionless form in Figs. 16 - 18. Figure 19 shows the dependency of the maximum velocity ratio that occurs with suction shroud (V/V_o) upon the characteristic ratios (A_0/A_2) and (a_1/a_2). This diagram can be used to get an estimate of the

maximum meridional velocity to be expected along the suction shroud of a radial flow impeller channel. For example, the impeller shroud profile of Fig. 2 is characterized by the ratios

$$A_0/A_2 = 0.57; \qquad a_1/a_2 = 1.2.$$

From Fig. 19 it is seen that the maximum relative meridional velocity on the front shroud should be about 1.28. A separate study of this impeller channel gave a value of 1.27 (Fig. 11) indicating the usefulness of this chart.

The use of Figs. 16 in conjunction with Fig. 19 allows the prediction of the shroud pressure or velocity distribution for practically any given impeller. This knowledge enables a rapid estimation of the meridian distribution of velocity within the shroud passage to be made.

VI. Acknowledgment

The writer and project staff would like to acknowledge the work of Mr. Marc Kampé de Feriet who made the electric analog studies for partial fulfillment of the requirements for an advanced degree.

Appendix I

Notation

a_1, a_2 - semi major and minor axes of shroud ellipses

A - area of impeller exit

b - impeller breadth at exit

C_p - static pressure coefficient = $(H_s - H_o)/V_o^2/2g$

H - head

R - radius of curvature of streamlines

r - radial coordinate

s - arc distance along stream surface measured from impeller exit

V - velocity

α - absolute flow direction - measured from a radial line

ϕ - flow rate coefficient, flow rate/exit area x $r_2\omega$

ζ - total head coefficient $(H_T - H_o)/V_o^2/2g$

Subscripts

0 - refers to inlet pipe

2 - refers to impeller exit

s - refers to static head

T - refers to total head

Appendix II

The flow net is a graphical procedure for obtaining potential flows between arbitrary surfaces. Since the flow net equations are to be found in most books on advanced hydraulics or turbomachinery, they will be only quoted here.

The method depends upon satisfying the condition of irrotationality along a potential line or surface (i.e., line normal to the stream lines). By a process of trial and error, the spacing and radius of curvature of the streamlines is adjusted to satisfy both this equation and the continuity equation.

The pertinent formula is

$$\frac{dV}{dn} = -\frac{V}{R}$$

where V is the meridional velocity, n the distance along a normal measured positive in the direction of R, and R is the radius of curvature of a streamline. The above equation has the solution

$$V = V_i \, e^{\int_o^n \frac{dn}{R(n)}}$$

which can be graphically integrated after an estimation of $R(n)$. The first estimation of $R(n)$ is corrected by requiring the increment of flow between any two streamlines to be constant. The velocity at the suction shroud (V_i) where $n = 0$ is determined by the fact that a given amount of discharge Q passes through the impeller, i.e., $Q = \pi R_o^2 V_o$. In this way the velocity distribution through the passage can be obtained after a few tries.

Often a satisfactory estimate can be obtained by approximating the function $1/R(n)$ with two or more terms in a power series.

References

1. Morelli, D. A., Osborne, W. C., "Head and Flow Observations on a High Efficiency Free Centrifugal Pump Impeller", Trans. ASME, Vol. 72, pp. 999-1006.

2. Osborne, W. C., Morelli, D. A., "Measured Performance of Pump Impellers", ASME Paper No. 50-A-90 (1950).

3. Morelli, D. A., Beveridge, J. H., "Evaluation of a Two-Dimensional Centrifugal Pump Impeller", ASME Paper No. 50-A-147 (1950).

4. Morelli, D. A., "Pressure Distribution on the Vanes of a Radial Flow Impeller", Trans. Heat Transfer and Fluid Mechanics Institute, 1950, p. 73, Stanford Univ. Press.

5. Acosta, A. J., "An Experimental and Theoretical Investigation of Two-Dimensional Centrifugal Pump Impellers", Report No. 21-9, Hydrodyanmics Laboratory, California Institute of Technology, 1952.

6. Acosta, A. J., Bowerman, R. D., "An Experimental Study of Centrifugal Pump Impellers", Hydrodynamics Laboratory, California Institute of Technology, unpublished.

7. Stepanoff, A. J., "Centrifugal and Axial Flow Pumps", Wiley, 1948.

8. Blom, C., "Development of the Hydraulic Design for the Grand Coulee Pumps", Trans. ASME, Vol. 72, pp. 93.

9. Knapp, R. T., "The Hydraulic Machinery Laboratory at the California Institute of Technology", Trans. ASME, Vol. 58, pp. 649-661.

10. Gongwer, C. A., "A Theory of Cavitation Flow in Centrifugal Pump Impellers", Trans. ASME, Vol. 63, No. 1, Jan. 1941.

11. de Feriet, M. K., "Investigation of Boundaries for Transitions from Axial to Two-Dimensional Flow by Electrical Analog", Mechanical Engineer Thesis, California Institute of Technology, 1953.

12. Binder, R. C., Knapp, R. T., "Experimental Determination of the Flow Characteristics in the Volutes of Centrifugal Pumps", Trans. ASME, Vol. 58, p. 649.

13. Acosta, A. J., "Note on the Effect of Meridian Curvature", Hydrodynamics Laboratory Report No. E-19.5, California Institute of Technology, May 1954.

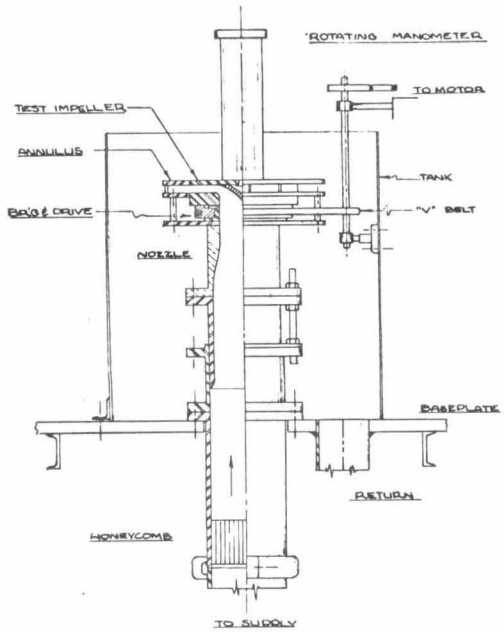

Fig. 1 - Impeller shroud assembly in test basin

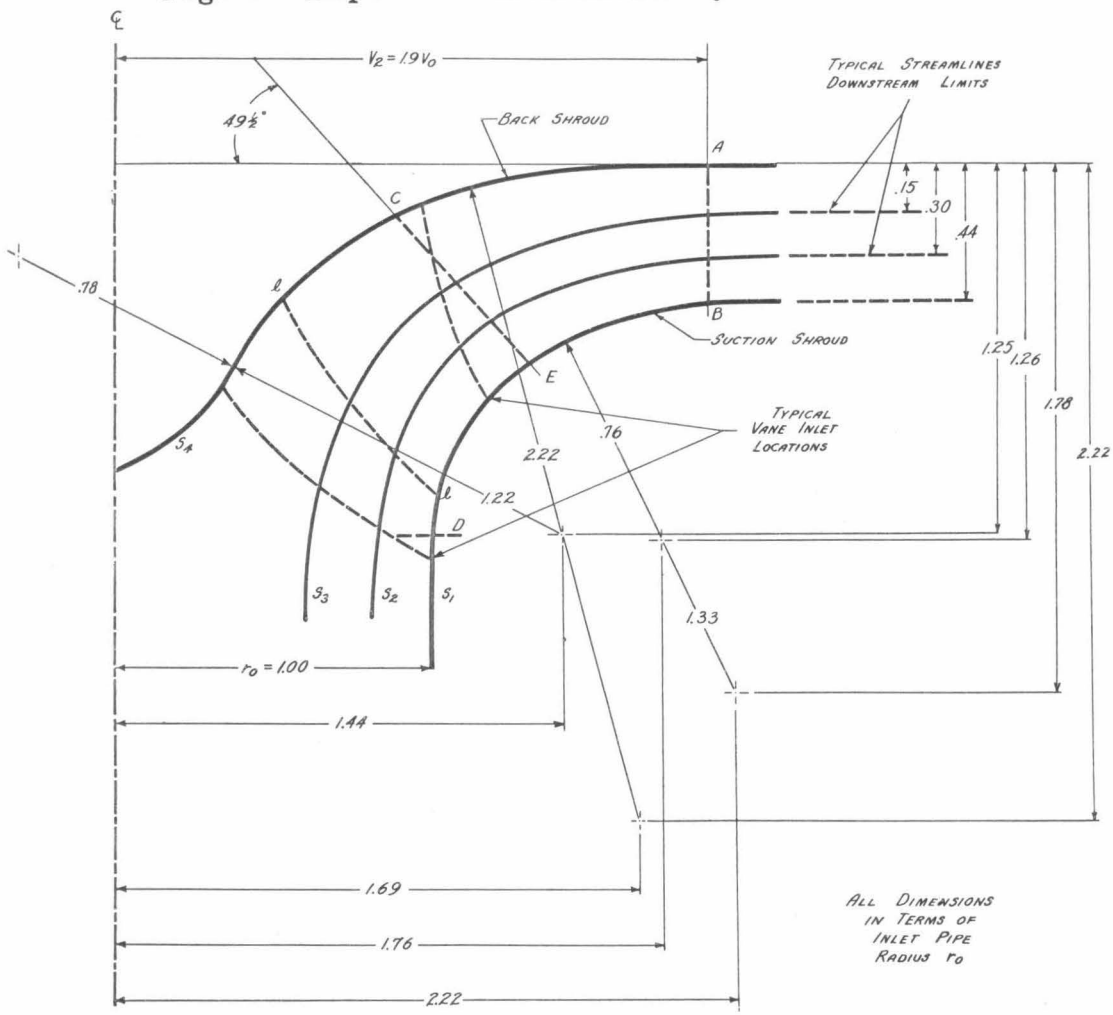

Fig. 2 - Impeller shroud profile geometry

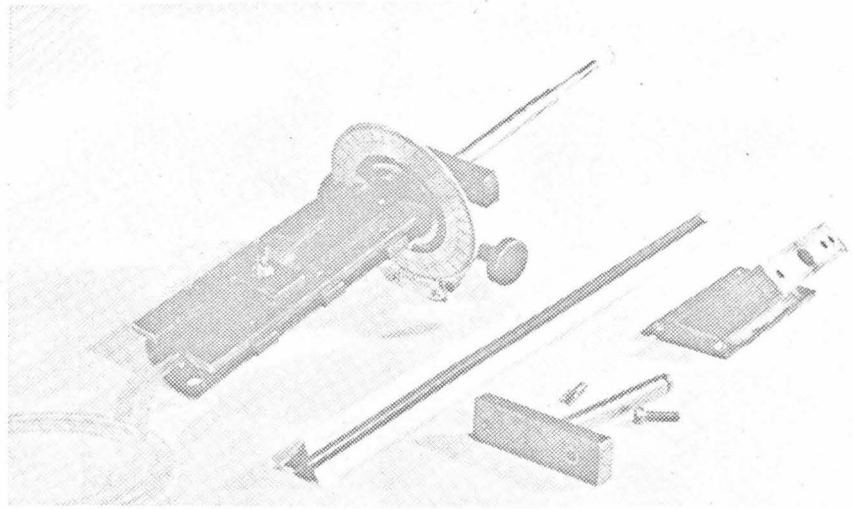

Fig. 3a - Probe holder

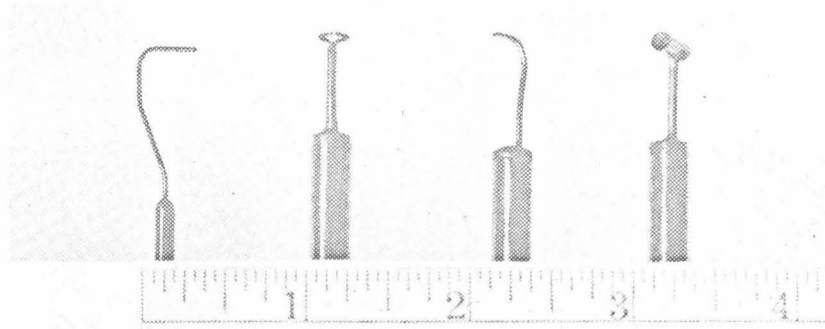

Fig. 3b - Miscellaneous probing devices

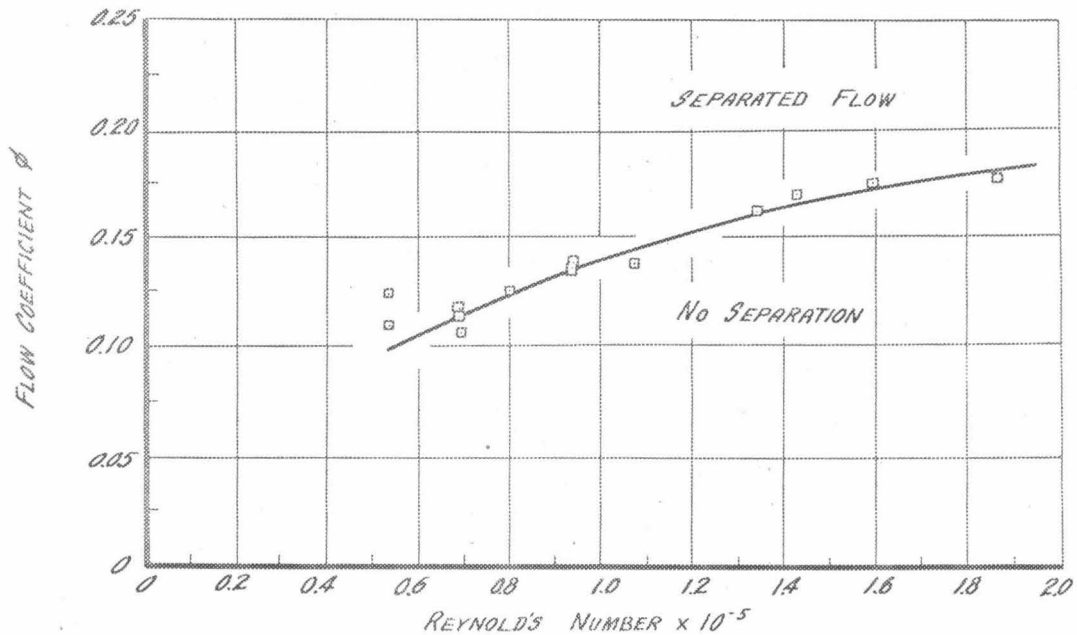

Fig. 4 - Flow coefficient necessary to suppress separation vs. Reynolds number

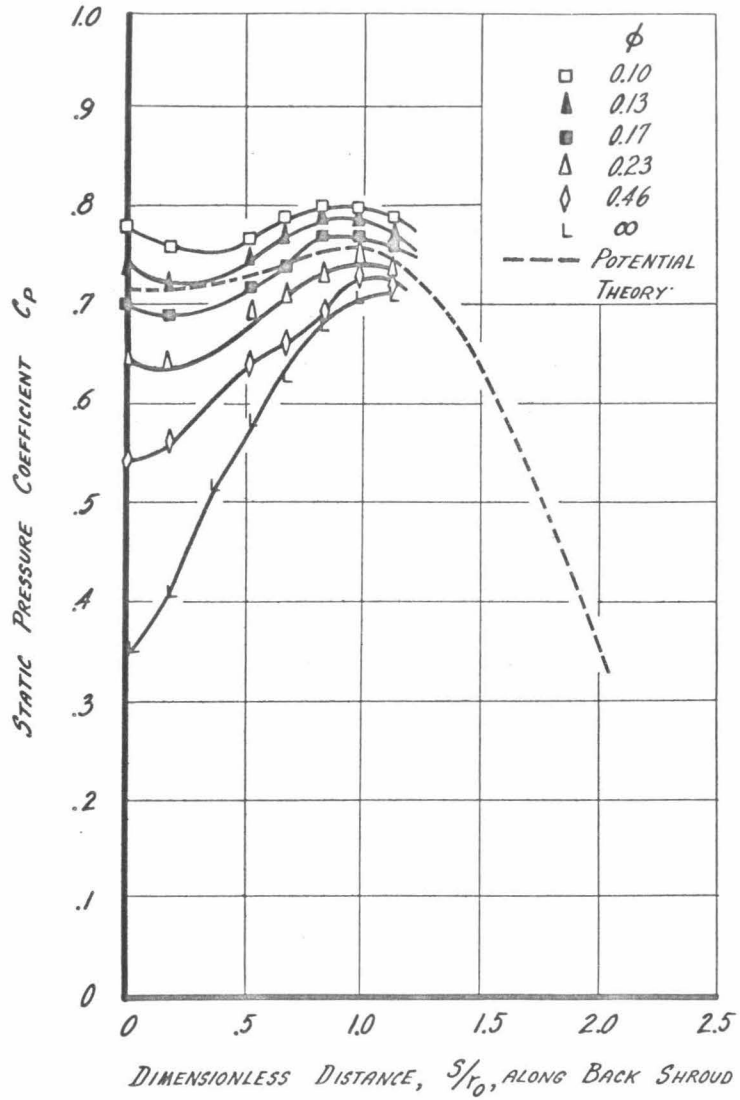

Fig. 5 - Distribution of pressure along impeller back shroud as a function of flow rate

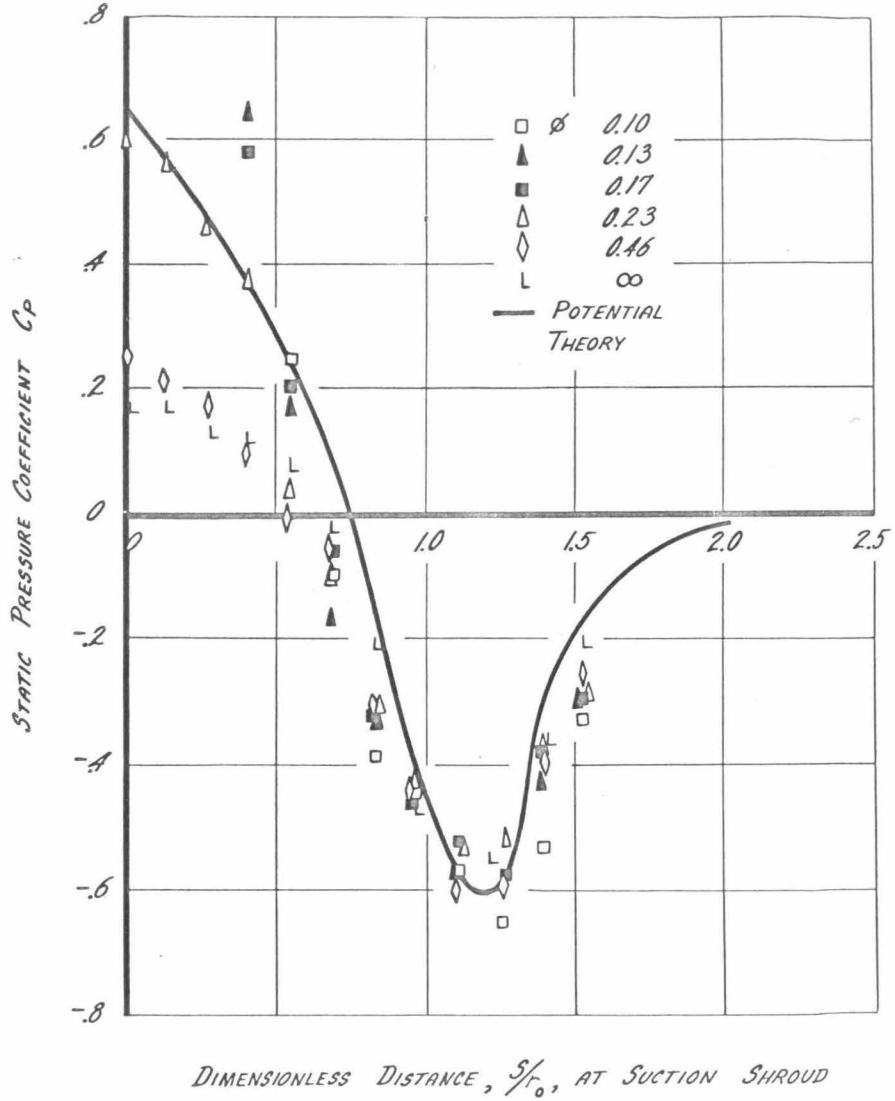

Fig. 6 - Distribution of pressure along impeller front or suction shroud as a function of flow rate

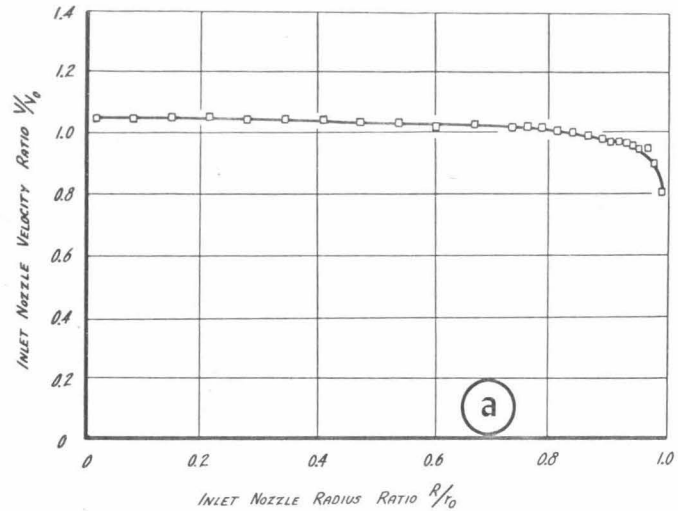

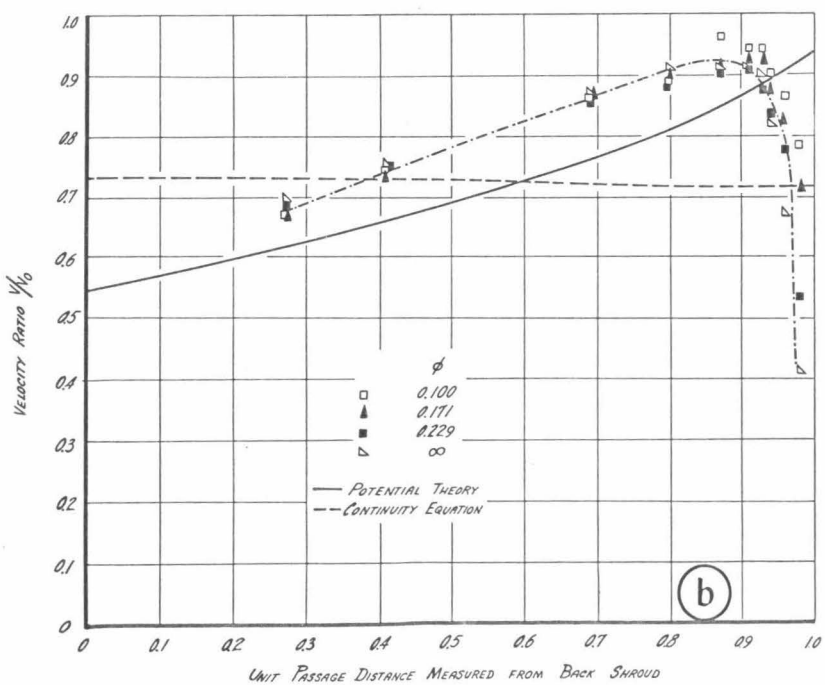

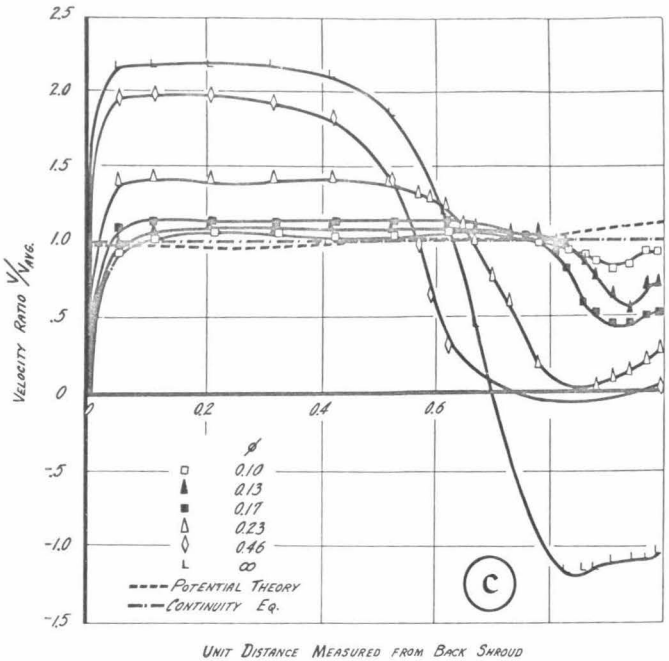

Fig. 7 - Meridional velocity distribution between impeller shrouds at three stations:
(a) nozzle throat
(b) intermediate station C-E
(c) impeller exit station A-B

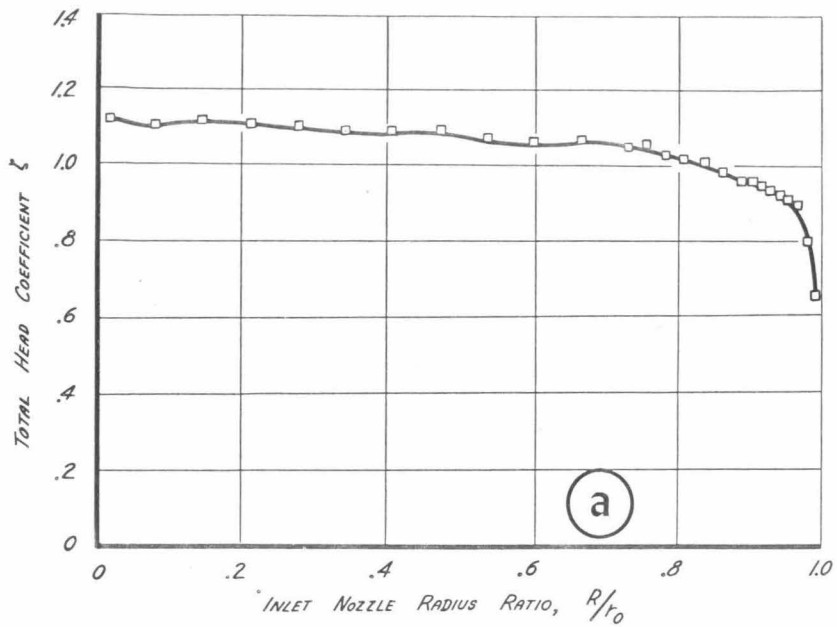

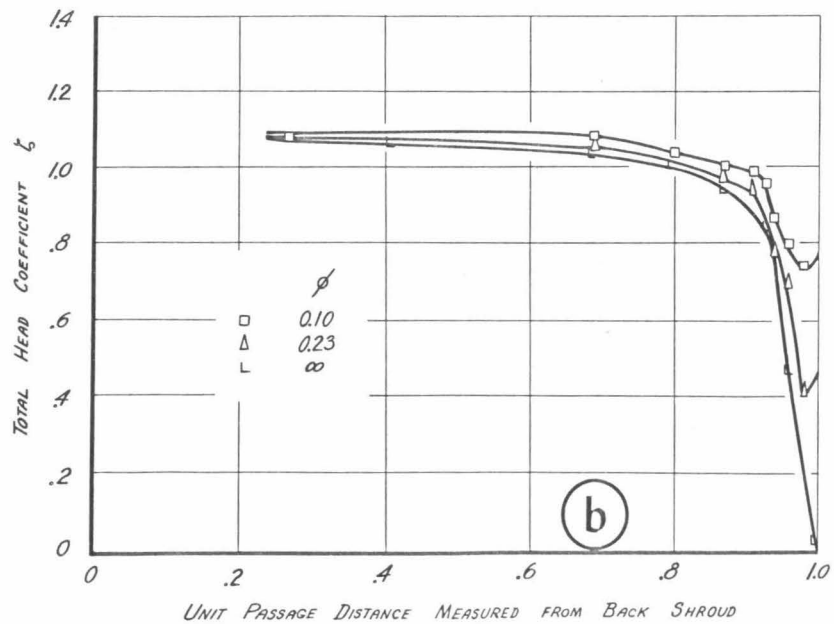

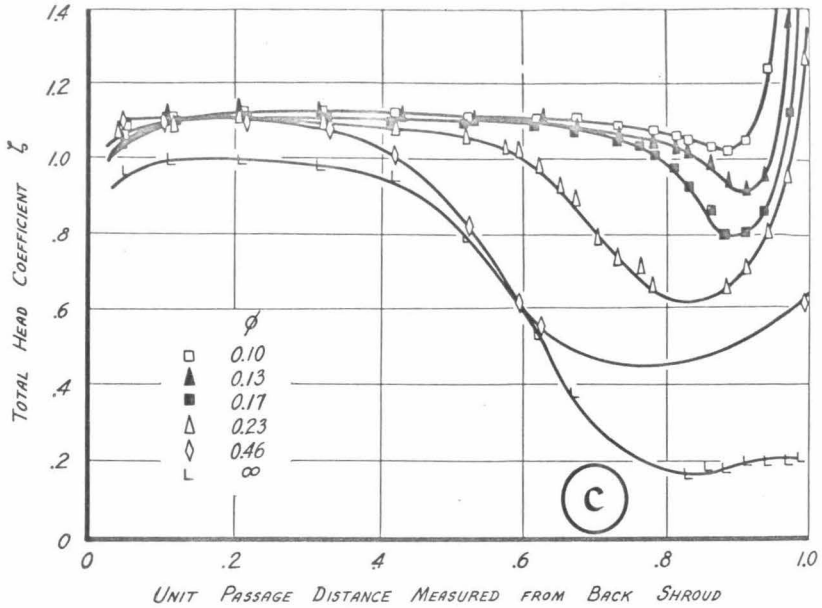

Fig. 8 - Total head survey between the shrouds
(a) nozzle throat
(b) station C-E
(c) impeller exit station A-B

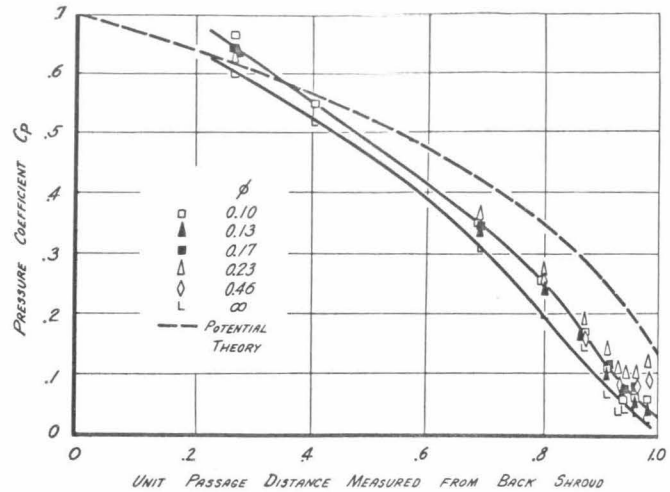

Fig. 9 - Distribution of static pressure across the passage at station C-E

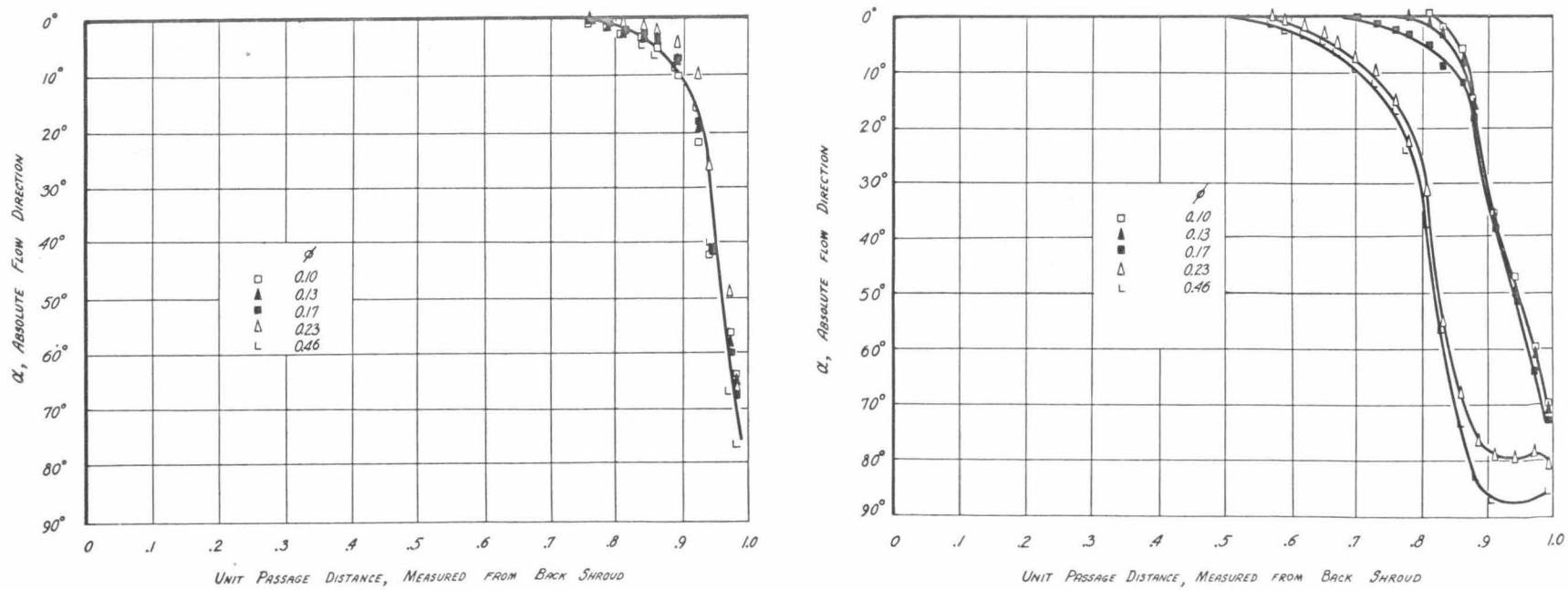

(a) station C-E

(b) impeller exit A-B

Fig. 10 - Influence of impeller suction shroud on direction of flow

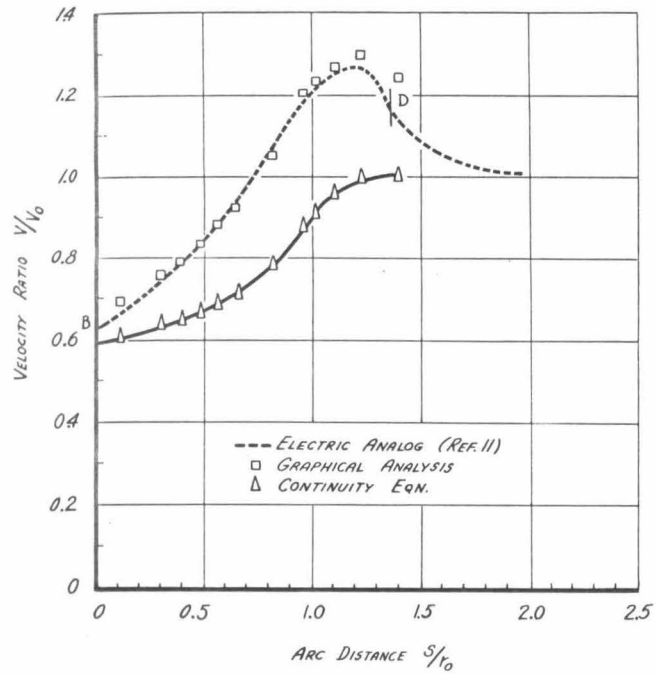

(a) streamline S_1

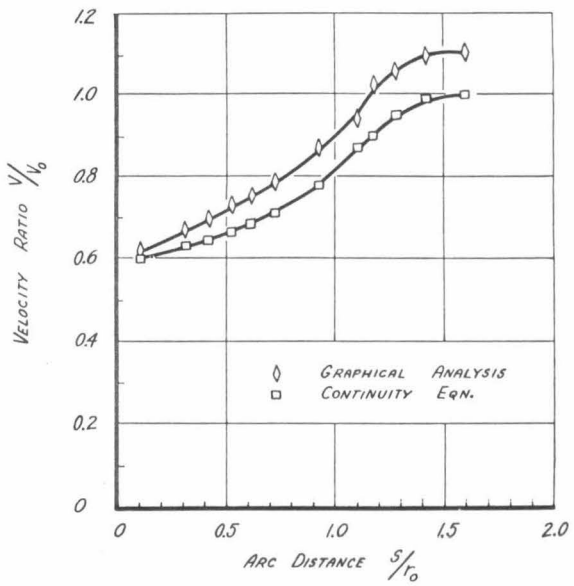

(b) streamline S_2

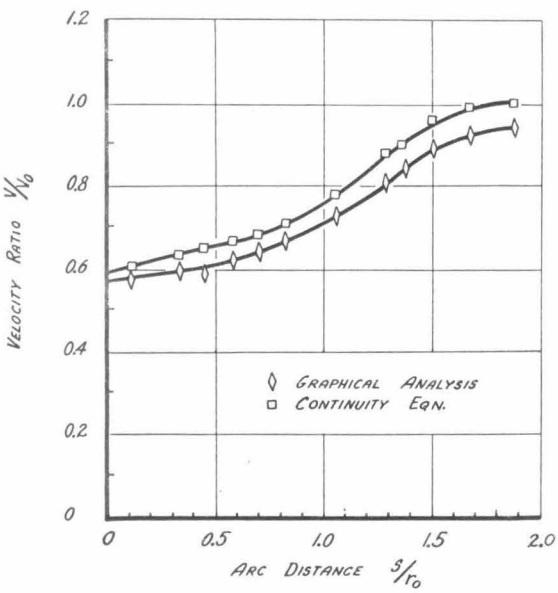

(c) streamline S_3

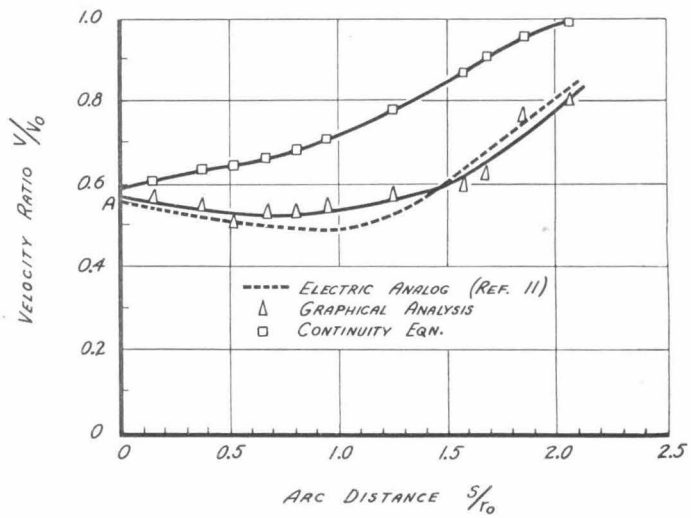

(d) streamline S_4

Fig. 11 - Theoretical meridional velocity distributions along several streamlines (see Fig. 2)

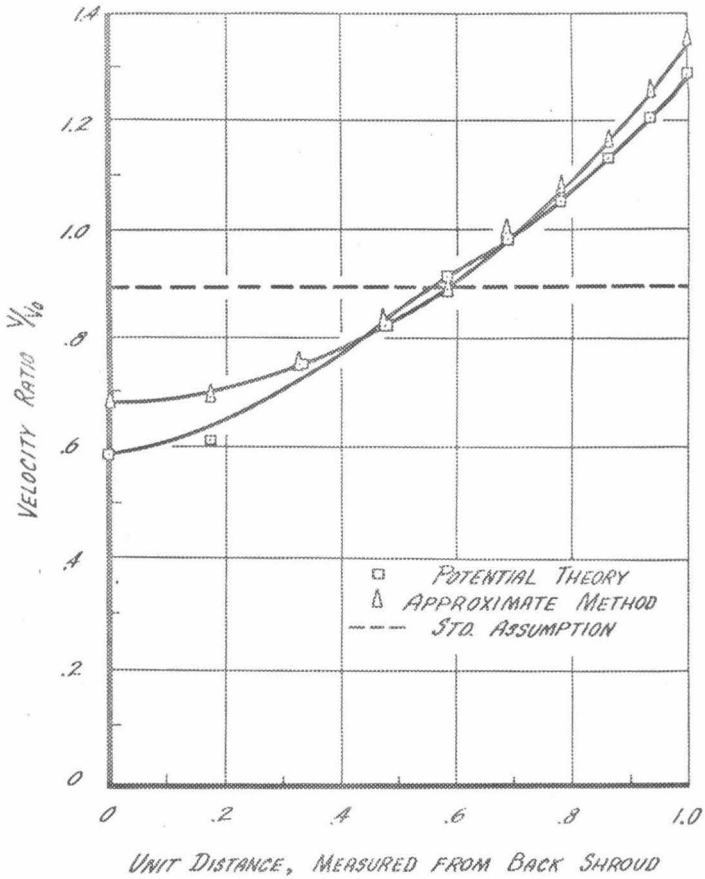

Fig. 12 - Theoretical velocity distribution along the vane inlet of a typical well-designed commercial impeller (line ℓ - ℓ in Fig. 2)

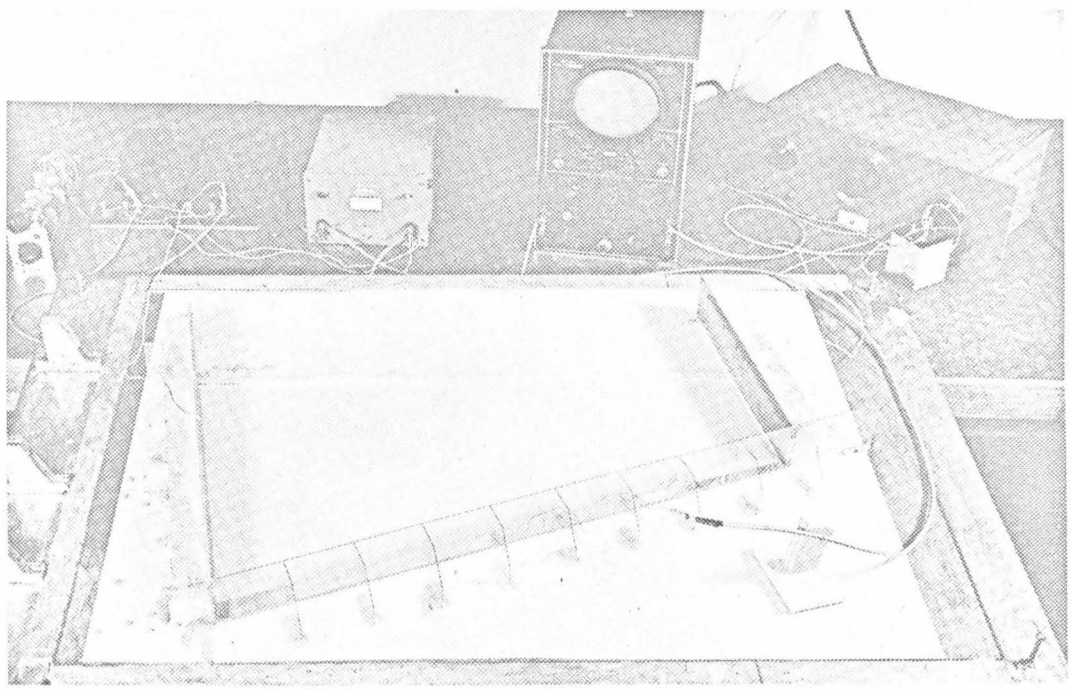

Fig. 13 - Photograph of electrolytic tank and equipment set up for a conical flow

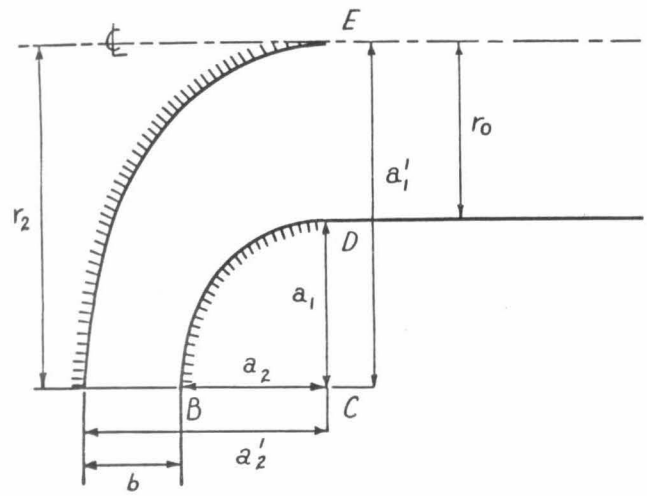

Fig. 14a - Sketch of shroud shapes used in analog studies

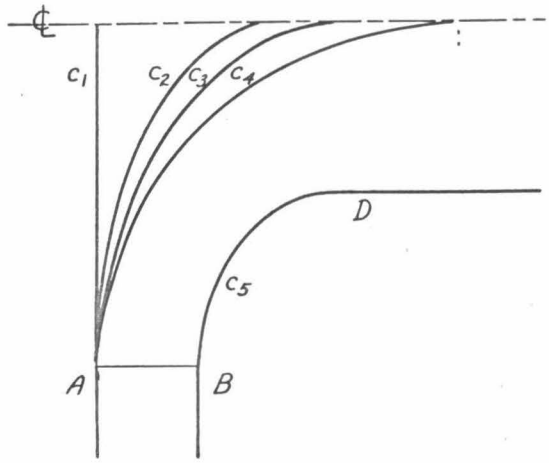

Fig. 14b - Back shroud curves used to determine effect on suction shroud

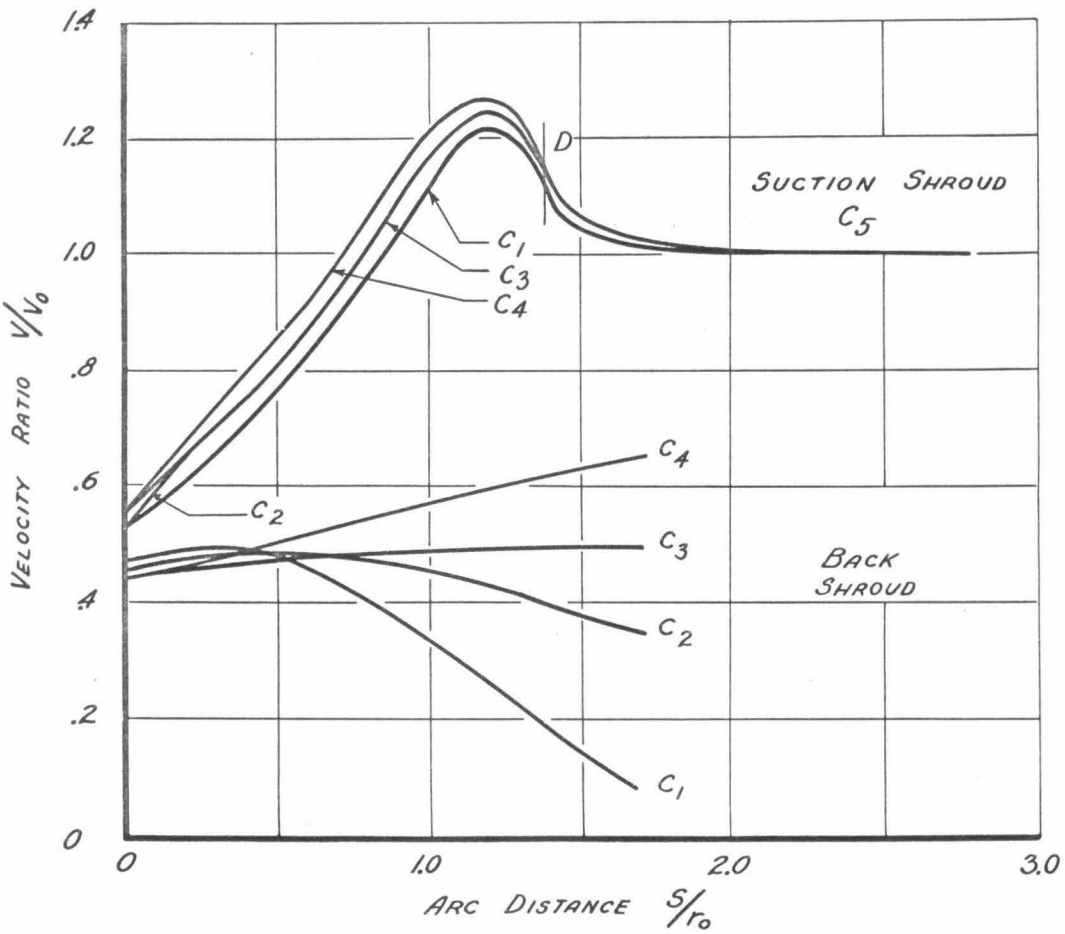

Fig. 15 - Effect of back shroud profile upon the meridional distribution of velocity on the suction shroud (see Fig. 14-b)

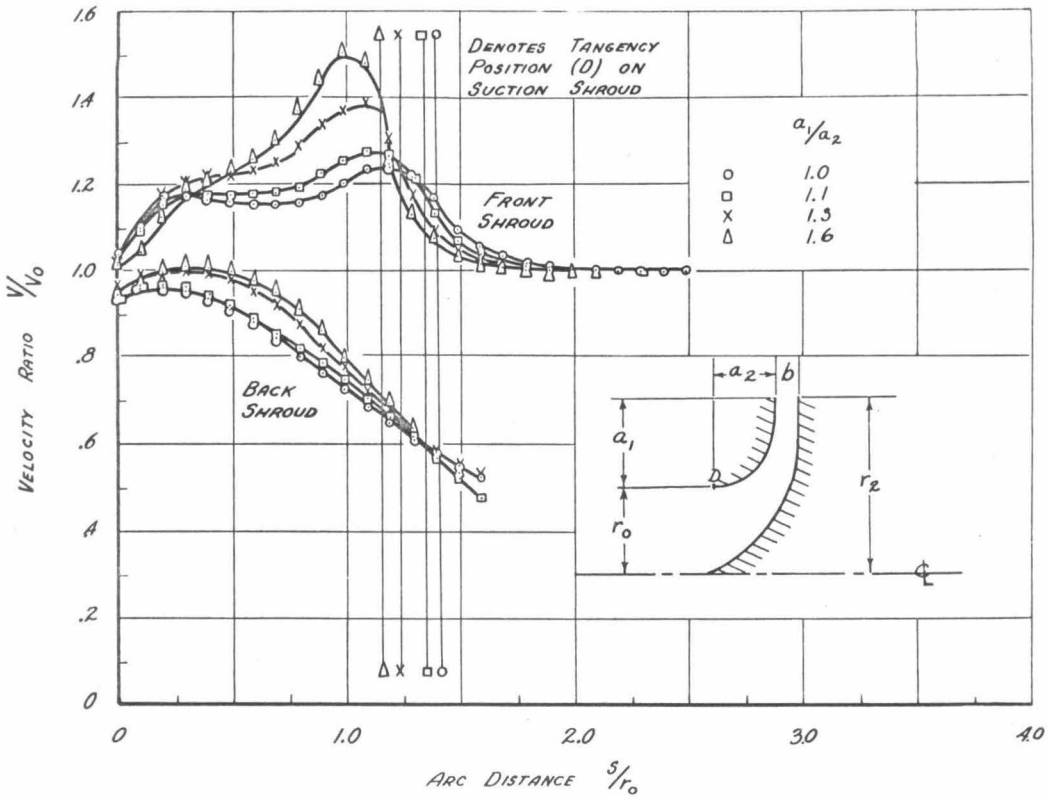

Fig. 16 - Velocity ratio vs. arc distance along shrouds for $r_2/r_0 = 1.9$, $A_0/A_2 = 1.0$ for various shroud eccentricities

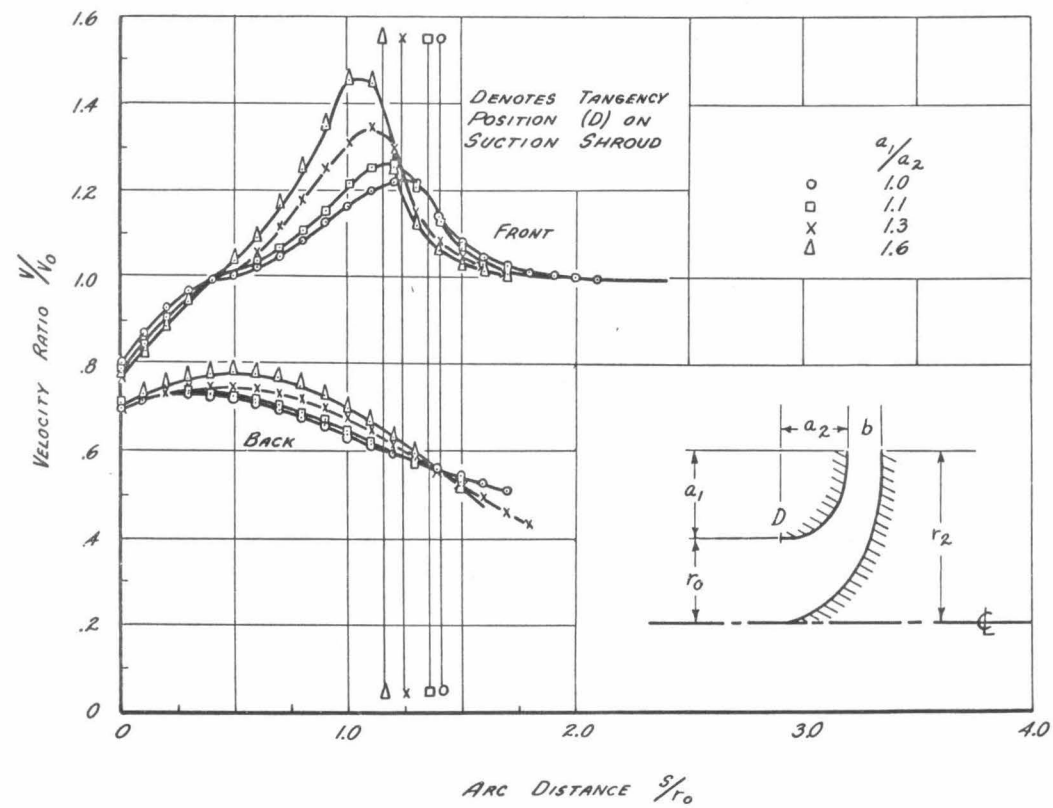

Fig. 17 - Velocity ratio vs. arc distance along shrouds for $r_2/r_0 = 1.9$, $A_0/A_2 = 3/4$

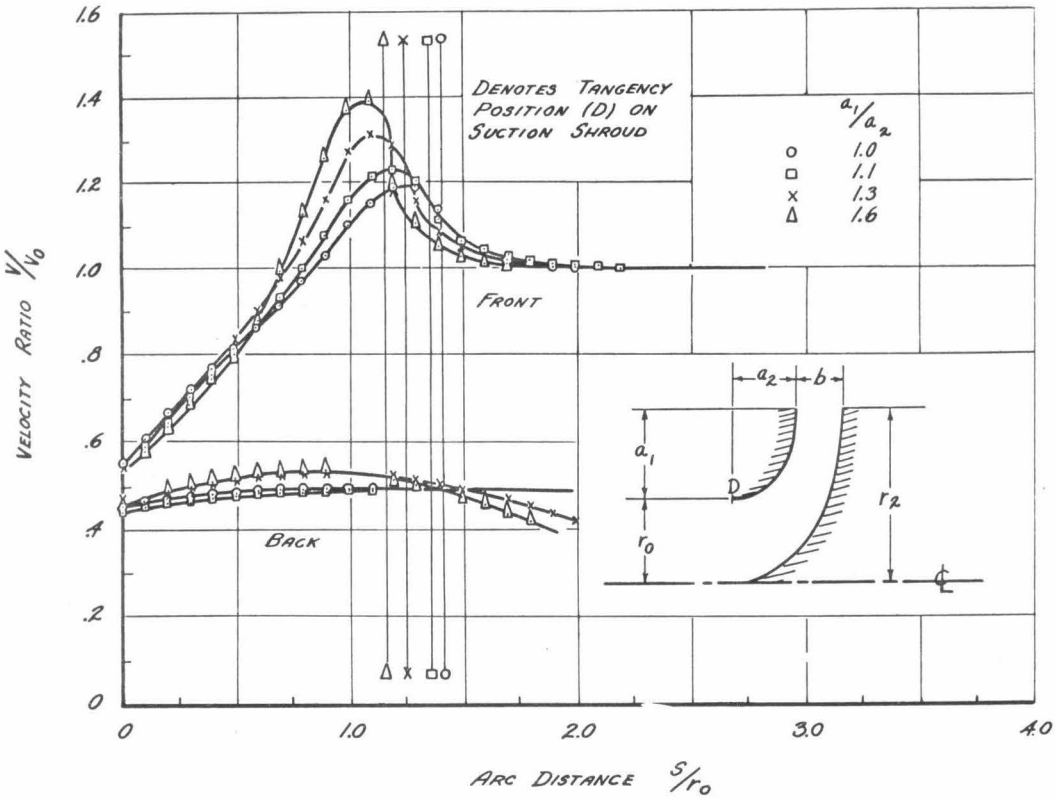

Fig. 18 - Velocity ratio vs. arc distance along shrouds for $r_2/r_0 = 1.9$, $A_0/A_2 = 1/2$

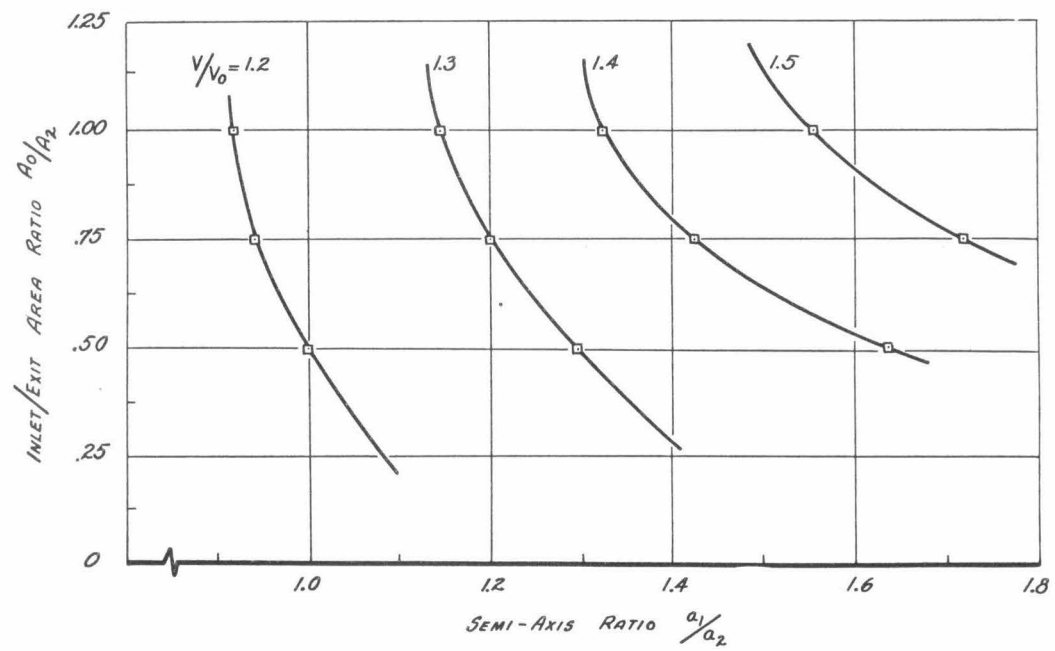

Fig. 19 - Peak meridian velocity on suction shroud as a function of the parameters A_0/A_2 and a_1/a_2

Addenda

The Reynolds number in these experiments is defined as

$$R_e = \frac{2r_o V_o}{\nu}$$

where

ν = kinematic viscosity

V_o = mean velocity in inlet pipe

r_o = radius of inlet pipe

The experiments were run at rotative speeds from 0-400 rpm and the inlet pipe diameter ($2r_o$) was 5.6 in.

It should be noted that these results, strictly speaking, do not apply to open (unshrouded) runners. However, in this case the centrifuging of the shroud boundary layer will be accomplished by the blades.

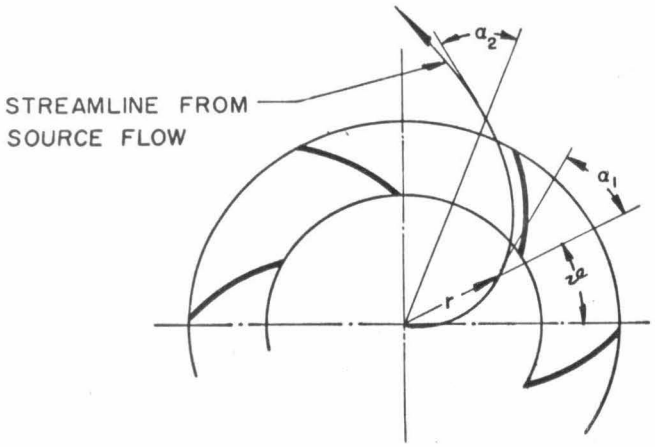

Fig. 3 - Definition sketch showing direction of positive α.

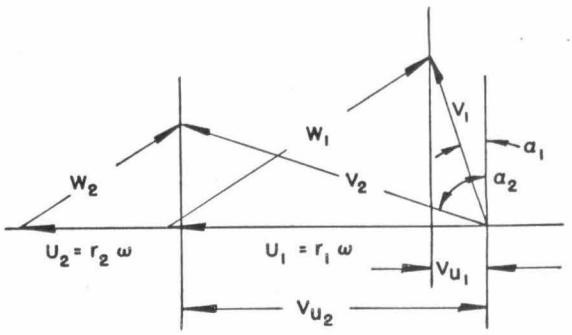

Fig. 4 - Definition sketch showing inlet and exit velocity triangles for backward curved vanes.

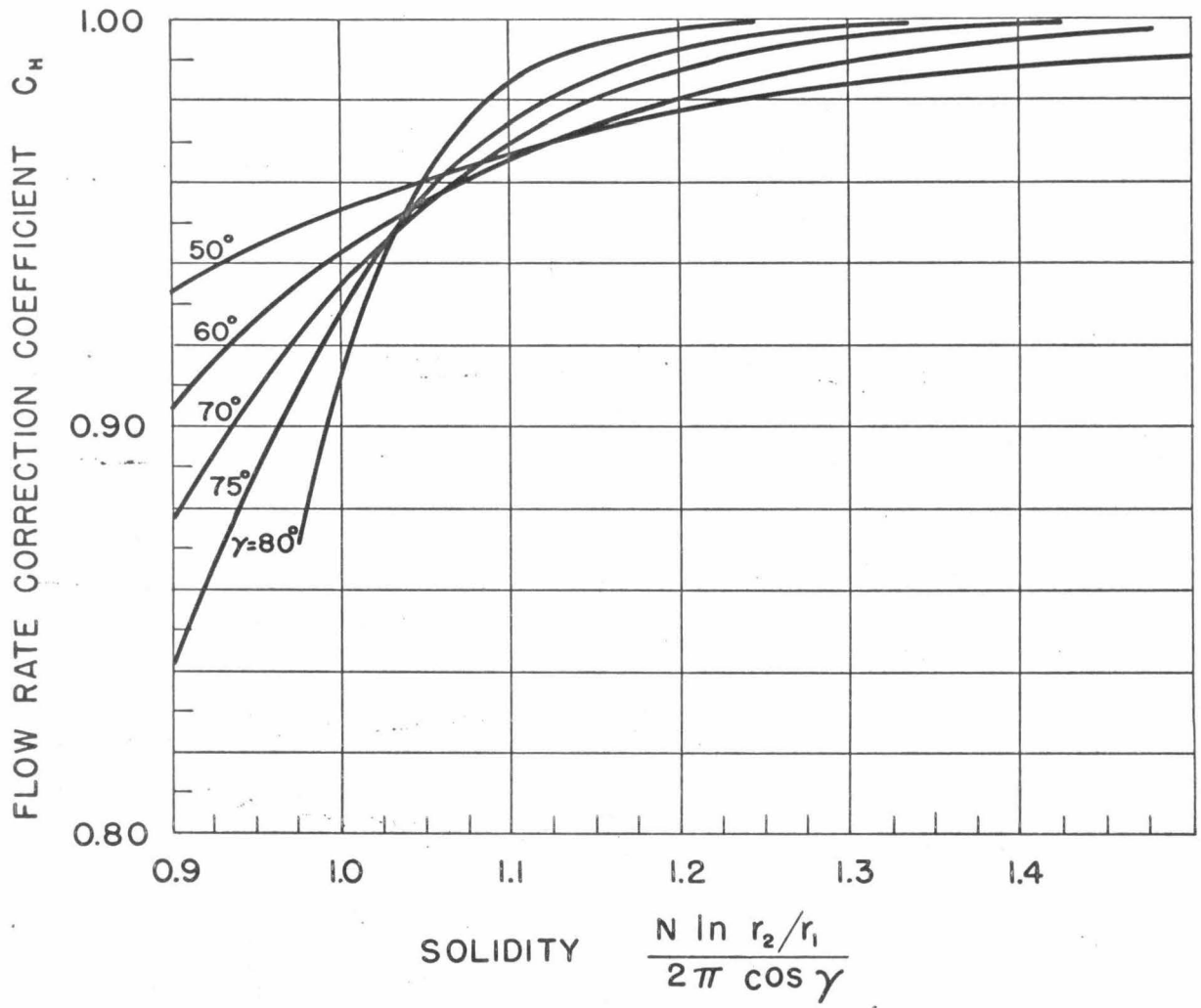

Fig. 5 - Correction factor C_H vs. solidity for various values of γ.

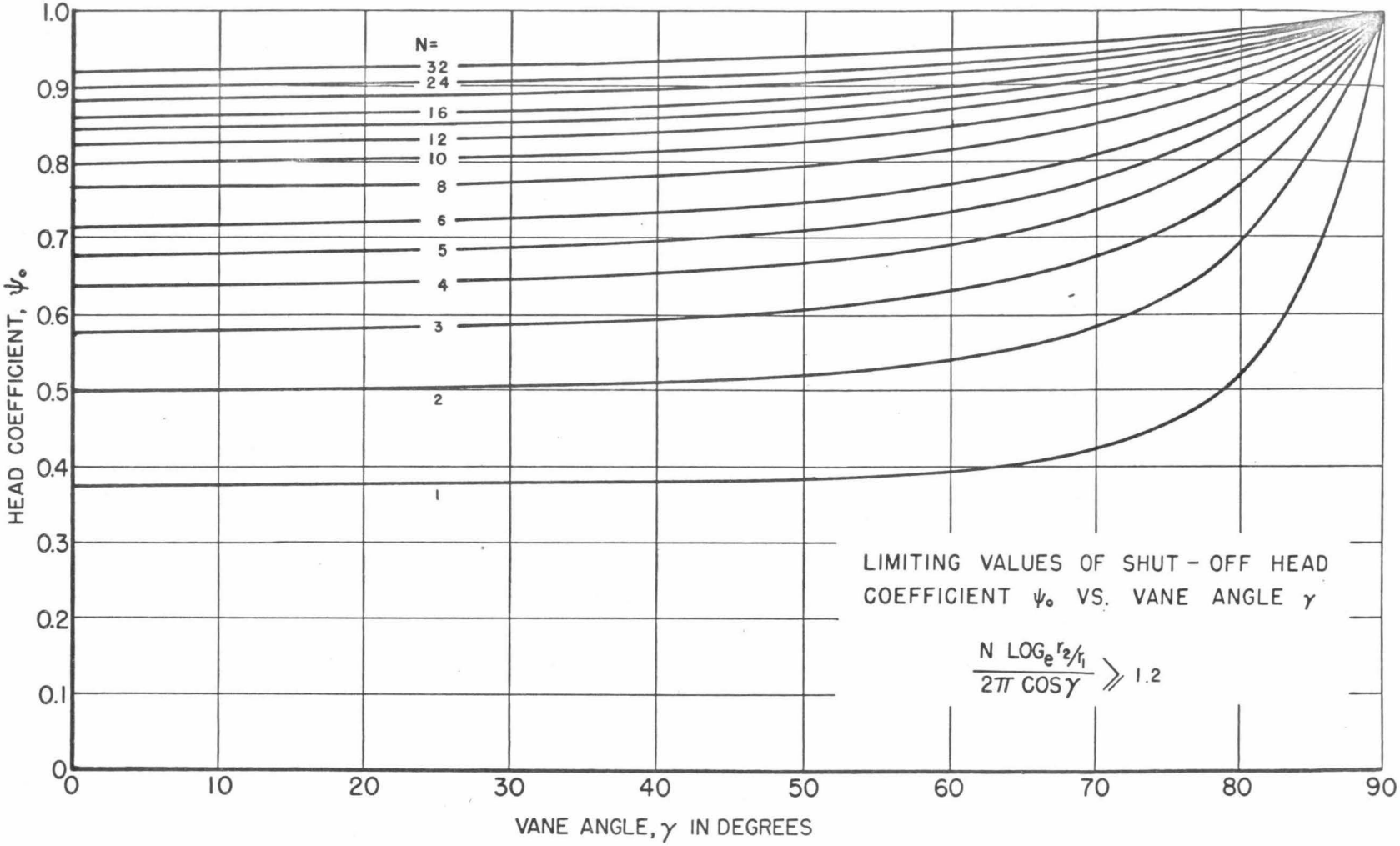

Fig. 6 - Limiting value of shut-off head coefficient ψ_o vs. stagger angle γ various values of N.

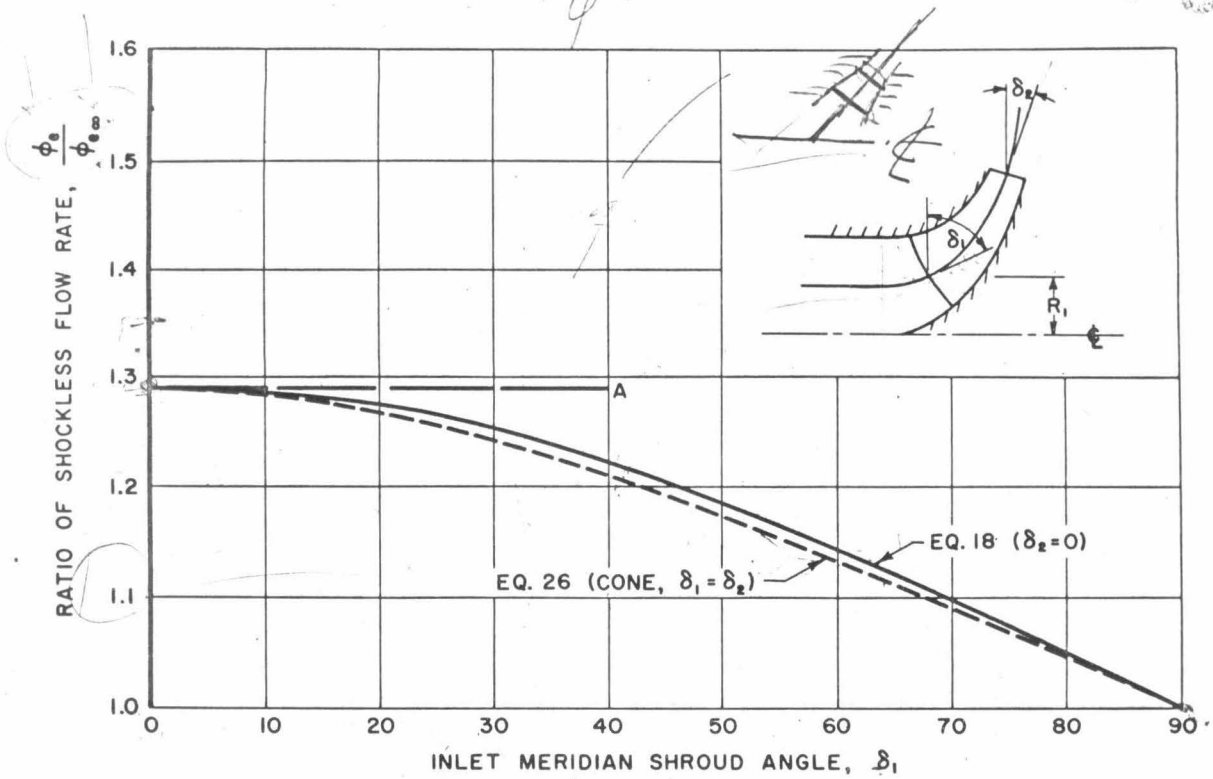

Fig. 5 - Ratio of shockless flow rates vs. inlet meridian shroud angle δ_1 for the case of 6 blades, $\gamma = 70^\circ$ and solidity = 1.2.

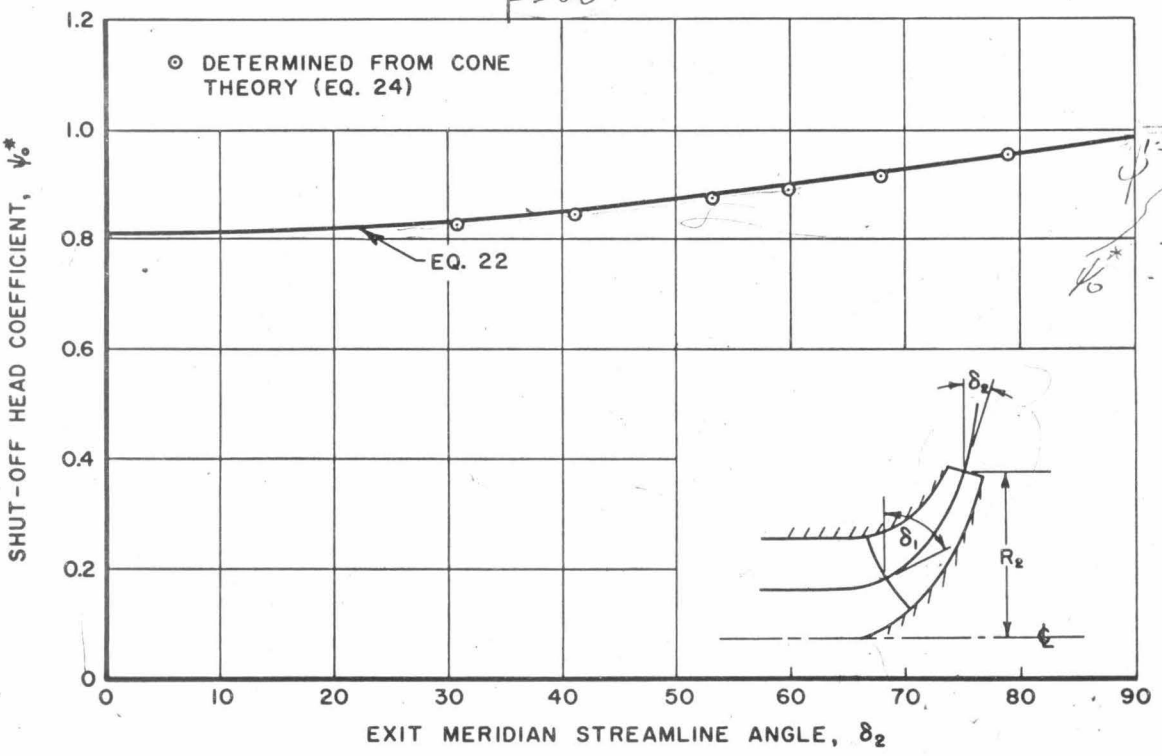

Fig. 6 - Shut-off head coefficient ψ_o^* vs. exit meridian shroud angle δ_2 for the case of 6 blades, $\gamma = 70^\circ$ and solidity = 1.2.